Turkish Journal of Electrical Engineering & Computer Sciences

http://journals.tubitak.gov.tr/elektrik/

Research Article

Turk J Elec Eng & Comp Sci
(2023) 31: 1 – 16

doi:10.55730/1300-0632.3967

# An adaptive image restoration algorithm based on hybrid total variation regularization

**Cong Thang PHAM**[1,*], **Thi Thu Thao TRAN**[2], **Hung Vi DANG**[3], **Hoai Phuong DANG**[1]

[1]The University of Danang - University of Science and Technology, Danang City, Viet Nam
[2]The University of Danang - University of Economics, Danang City, Viet Nam
[3]The University of Danang - University of Science and Education, Danang City, Vietnam

**Received:** 02.08.2022 • **Accepted/Published Online:** 31.10.2022 • **Final Version:** 19.01.2023

**Abstract:** In imaging systems, the mixed Poisson-Gaussian noise (MPGN) model can accurately describe the noise present. Total variation (TV) regularization-based methods have been widely utilized for Poisson-Gaussian removal with edge-preserving. However, TV regularization sometimes causes staircase artifacts with piecewise constants. To overcome this issue, we propose a new model in which the regularization term is represented by a combination of total variation and high-order total variation. We study the existence and uniqueness of the minimizer for the considered model. Numerically, the minimization problem can be efficiently solved by the alternating minimization method. Furthermore, we give rigorous convergence analyses of our algorithm. Experiments results are provided to demonstrate the superiority of our proposed hybrid model and algorithm for deblurring and denoising images simultaneously, in comparison with several state-of-the-art numerical algorithms.

**Key words:** Total variation, image restoration, mixed noise, minimization method

## 1. Introduction

Image restoration is a fundamental problem in digital image processing. The aim of image restoration is to reconstruct a good approximation of original $X$ from observed image $G$ and to preserve local image features for accurate and effective subsequent analysis. Images are corrupted by noise due to several causes including quality of transceivers, influence of light sources or environment conditions [1–4]. In various applications such as medicine, biology, astronomy, etc. [5–7], mixed Poisson-Gaussian noise (MPGN) model can accurately describe the noise present. In this model, Poisson components account for the uncertainty of signal dependence inherent in the photon counting process, while the white Gaussian noise additive component treats other noise sources independently of signals such as thermal noise [8]. In this problem, the image degradation process is modeled as $G = P_{\mathcal{P}}(X) + \mathcal{N}(0, \sigma^2)$, where $P_{\mathcal{P}}(X)$ represents the image $X$ degraded by Poisson noise and $\mathcal{N}(0, \sigma^2)$ represents Gaussian noise with zero mean and variance $\sigma$.

In the literature, several methods have been proposed for MPGN removal [9–13], e.g., approaches based on PURE-LET [3], variance stabilization transforms [14], unbiased risk estimator [10], contourlet transform and hidden Markov models [15]. Alternatively, methods based on total variation (TV) regularization also have been proposed for mixed Poisson-Gaussian noise removal, e.g., approach based on a TV regularization term and an infimal convolution modeling of the data discrepancies[16], a nonsmooth PDE-constrained optimization

*Correspondence: pcthang@dut.udn.vn

approach for the determination of the correct noise model [17], total variation regularization term and two data fidelity terms with the Kullback-Leibler divergence term for Poisson noise and the $L_2$ norm fidelity term for Gaussian noise [8], the Lipschitz differentiability and convexity of the Poisson-Gaussian neg-log-likelihood [6].

One of the popular approaches for image restoration is TV-based method. The TV based model for the mixed Poisson-Gaussian noise removal (MPGTV) has the following form [13]:

$$X^* = \underset{X \in S(\Omega)}{\arg\min} \int_\Omega |\nabla X| \, dt + \frac{\lambda_1}{2} \int_\Omega (X - G)^2 dt + \lambda_2 \int_\Omega (X - G \log X) dt, \tag{1}$$

where $G = G(t)$ is the known image, $t = (i; j) \in \Omega, i = 1 \dots M,\ j = 1 \dots N,\ \Omega \subset \mathbb{R}^2$ is an actual image domain, and $S(\Omega)$ is the set of positive functions from $\Omega$ to $\mathbb{R}$; $\lambda_1, \lambda_2$ are positive regularization parameters, $\int_\Omega |\nabla X| dt$ is the total variation of $X$, and $\nabla$ is gradient operator.

The model (1) is effective in removing MPGN. Unfortunately, this model has a staircase artifact, i.e. smooth regions that are transformed into piecewise constant areas. This effect leads to develop false edges that do not exist in the true image [18]. To avoid the staircase effect, many approaches in the literature were made to replace the TV norm with the high-order TV norm [19–21]. The popular type of the high-order TV norms is second-order derivative $\nabla^2$ [21–23]. However, the methods using the second-order often lead to the edges blurring in obtained results.

To avoid the above issues, we consider to add a second-order functional to the total variation model (1) for restoring images corrupted by MPGN as follows:

$$X^* = \underset{X \in S(\Omega)}{\arg\min} \left( \int_\Omega \gamma(t) \, |\nabla X| \, dt + \int_\Omega (1 - \gamma(t)) \, |\nabla^2 X| dt + \frac{\lambda_1}{2} \int_\Omega (X - G)^2 dt + \lambda_2 \int_\Omega (X - G \log X) dt \right), \tag{2}$$

where $\lambda_1, \lambda_2$ are positive regularization parameters, $S(\Omega)$ is the set of positive functions from $\Omega$ to $\mathbb{R}$, $\gamma(t)$ is the edge-stopping function defined later in (14), and $\nabla^2$ is second-order derivative. In this work, we study both deblurring and denoising simultaneously. In case of the blur effect, we can generalize the proposed model (2) for restoring a blurred image corrupted by MPGN as follows:

$$X^* = \underset{X \in S(\Omega)}{\arg\min} E(X), \tag{3}$$

$$E(X) = \left( \int_\Omega \gamma(t) \, |\nabla X| \, dt + \int_\Omega (1 - \gamma(t)) \, |\nabla^2 X| dt + \frac{\lambda_1}{2} \int_\Omega (\mathcal{H}X - G)^2 dt + \lambda_2 \int_\Omega (\mathcal{H}X - G \log \mathcal{H}X) dt \right),$$

where $\mathcal{H}$ stands for a linear blurring operator.

The main contributions of this work are the following: We proposed an adaptive model for MPGN removal problem. It is easy to see that when $\gamma(x) = 1$, we obtain the model (1). Thus, our model can keep keen edges like model (1). Our model efficiently combines the advantage of the TV denoising model and the second-order TV denoising model. This allows to suppress the MPGN efficiently, preserve edges of object in the piecewise constant image, and alleviate staircase artifacts in the obtained images. We prove the existence and uniqueness of minimizer for proposed model. Since the proposed model has the splitting frame, we establish an alternating minimization method to solve the minimization problem. We study the convergence property of the algorithm. Numerical experiments are provided to demonstrate the high efficiency of our algorithm for recovering images corrupted by MPGN.

The rest of the paper is organized as follows: In Section (2), we describe the necessary definitions and notations on the considered model. In Section (3) we describe the proposed optimization framework. Next, in Section (4), we show some numerical results of our proposed method and we compare them with the results obtained with other existing and well-known methods. Finally, some conclusions are drawn in Section (4).

## 2. Preliminaries

Our goal is to recover the original image $X$ with given (observed) image $G$. The problem is to find the image $X$ so that the conditional probability $\mathcal{P}(X|G)$ can be maximized. Using Bayes's rule, we have:

$$\mathcal{P}(X|G) = \frac{\mathcal{P}(G|X)\mathcal{P}(X)}{\mathcal{P}(G)}. \tag{4}$$

The Poisson noise and the Gaussian noise are independent of each other; therefore, the distribution of MPGN can be expressed as follows:

$$\mathcal{P}(G|X) = \prod_{\imath\in\mathcal{I}} P_{\mathcal{P}}(G_\imath|X_\imath)\cdot P_{\mathcal{N}}(G_\imath|X_\imath), \tag{5}$$

where $\mathcal{I}$ denotes the domain of $G$, $P_{\mathcal{N}}(G|X) = \frac{1}{\sigma\sqrt{2\pi}}\exp\left(-\frac{(X-G)^2}{2\sigma^2}\right)$ and $P_{\mathcal{P}}(G|X) = \frac{X^G\exp(-X)}{G!}$.

Motivated by the TV models, $\mathcal{P}(X)$ follows a Gibbs prior [2]:

$$P(X) = \frac{1}{\mathcal{Z}}\exp(-\int \phi(X)dt), \tag{6}$$

where $\mathcal{Z}$ is a normalization factor, $\phi(X) = \gamma|\nabla X| + (1-\gamma)|\nabla^2 X|$.

The estimation $\max\mathcal{P}(X|G)$ can be equivalently expressed as minimization problem by considering the logarithmic transformation $\min\Big(-\log(\mathcal{P}(G|X)) - \log(\mathcal{P}(X))\Big)$. Thus, we can plug in Equations (5) and (6) to get the TV-based model for MPGN removal (MPGTV) in (2):

$$X^* = \arg\min_{X\in S(\Omega)} \int_\Omega \gamma(t)\,|\nabla X|\,dt + \int_\Omega (1-\gamma(t))\,\left|\nabla^2 X\right|dt + \frac{\lambda_1}{2}\int_\Omega (X-G)^2 dt + \lambda_2\int_\Omega (X - G\log X)dt.$$

In case of the blur effect, we have form of the proposed model for restoring a blurred image corrupted by MPGN in Eq. (3):

$$X^* = \arg\min_{X\in S(\Omega)} E(X),$$

$$E(X) = \left(\int_\Omega \gamma(t)\,|\nabla X|\,dt + \int_\Omega (1-\gamma(t))\,|\nabla^2 X|dt + \frac{\lambda_1}{2}\int_\Omega (\mathcal{H}X-G)^2 dt + \lambda_2\int_\Omega (\mathcal{H}X - G\log\mathcal{H}X)dt\right).$$

Referring [24–26], we briefly review some necessary definitions and notions for the proposed model.

**Definition 1** *Let $\Omega\subset\mathbb{R}^n, n\geq 2$ be an open, bounded Lipschitz domain. Let $X\in L^1(\Omega)$. Then the total variational of $X$ is defined by:*

$$\int_\Omega |\nabla X| = \sup\left\{\int_\Omega X div(\vartheta)dx : \vartheta\in\mathcal{C}_c^1(\Omega,\mathbb{R}^n), |\vartheta|\leq 1\right\},$$

where $\mathcal{C}_c^1(\Omega, \mathbb{R}^n)$ denotes continuously differentiable vector functions of compact support contained in $\Omega$, and the space of functions of bounded variation $BV(\Omega)$ is equipped with the norm $|X|_{BV(\Omega)} = |X|_{L^1(\Omega)} + \int_\Omega |\nabla X|$.

**Definition 2** *Let $\Omega \subset \mathbb{R}^n, n \geq 2$ be an open, bounded Lipschitz domain. Let $X \in L^1(\Omega)$. Then the $BV^2$ seminorm of $X$ is defined by:*

$$\int_\Omega |\nabla^2 X| = \sup \left\{ \int_\Omega \Sigma_{i,j=1}^n X \partial_j \partial_i \vartheta^{ij} dt : \vartheta \in \mathcal{C}_c^2(\Omega, \mathbb{R}^{n\times n}), |\vartheta| \leq 1 \right\},$$

where $|\vartheta| = \sqrt{\Sigma_{i=1}^n \Sigma_{j=1}^n (\vartheta^{ij})^2}$ and $BV^2(\Omega)$ is equipped with the norm $|X|_{BV^2(\Omega)} = |X|_{L^1(\Omega)} + \int_\Omega |\nabla^2 X|$.

**Definition 3** *Let $\Omega \subset \mathbb{R}^n, n \geq 2$ be an open, bounded Lipschitz domain. Let $X \in L^1(\Omega)$ and $\alpha(t) \geq 0$. Then space $\alpha - BV$ seminorm of $X$ is defined by:*

$$\int_\Omega \alpha |\nabla X| = \sup \left\{ \int_\Omega X div(\vartheta) dt : \vartheta \in \mathcal{C}_c^1(\Omega, \mathbb{R}^n), |\vartheta_i| \leq \alpha, 1 \leq i \leq n \right\},$$

where $\vartheta = (\vartheta_1, \vartheta_2, ...\vartheta_n)$ and the space $\alpha - BV(\Omega)$ norm is $|X|_{BV(\Omega)} = |X|_{L^1(\Omega)} + \int_\Omega \alpha |\nabla X|$.

**Definition 4** *Let $\Omega \subset \mathbb{R}^n, n \geq 2$ be an open, bounded Lipschitz domain. Let $X \in L^1(\Omega)$ and $\beta(t) \geq 0$. Then space $\beta - BV^2$ seminorm of $X$ is defined by:*

$$\int_\Omega \beta |\nabla^2 X| = \sup \left\{ \int_\Omega \Sigma_{i,j=1}^n X \partial_j \partial_i \vartheta^{ij} dt : \vartheta \in \mathcal{C}_c^2(\Omega, \mathbb{R}^{n\times n}), |\vartheta| \leq \beta \right\}$$

and the $\beta - BV^2(\Omega)$ norm is $|X|_{\beta - BV^2(\Omega)} = |X|_{L^1(\Omega)} + \int_\Omega \beta |\nabla^2 X|$.

We can realize that our objective function (3) is defined on $S(\Omega) = \{X \in BV(\Omega) \cap BV^2(\Omega), X > 0\}$. We study the existence and uniqueness of the minimizer for proposed problem as follows.

**Theorem 1** *Let $\inf G > 0$ and $\mathcal{H}$ be injective, then a solution of the problem (3) is unique minimizer.*

**Proof** The proof is similar to the proof of [27, 28]. Let $X^{(k)}$ be a bounded minimizing sequence. By the compactness property in the space of bound variation $BV(\Omega)$ and $BV^2(\Omega)$ [25, 27, 29], there exists $X^* \in BV(\Omega) \cap BV^2(\Omega)$, such that $X^{(k)}$ converges weakly to $Z^* \in BV(\Omega) \cap BV^2(\Omega)$ and $Z^{(k)}$ converges strongly to $Z^*$ in $L^1(\Omega)$. Thus, $X^*$ is the minimizer of model (3) for all $X \in BV(\Omega) \cap BV^2(\Omega)$ such that $\log X \in L^1(\Omega)$. Furthermore, $\mathcal{H}$ is positive definite and $G$ is positive, the total variation terms are convex, hence $E(X)$ is strongly convex. According to Fatou's lemma [30], we have: $E(X) \geq E(X^*)$. Thus, $X^*$ is unique minimizer of the optimization problem (3). □

## 3. Computational method

There are many methods which can be employed to obtain the solution of the optimization problem (3), for instance, the primal-dual algorithm [31], the split Bregman algorithm [32], alternating minimization method [33–35]. In this article, we decide to employ the alternating minimization method for solving the optimization

problem (3). Following the popular alternating minimization method [36, 37], by introducing three new variables $(D, Q, Z)$, the model (3) can be reformulated as the following constrained optimization problem:

$$\min_{Z,D,Q} \left( \gamma \|D\|_1 + (1-\gamma)\|Q\|_1 + \frac{\lambda_1}{2}\|Z - G\|_2^2 + \lambda_2 \langle 1, Z - G\log Z \rangle \right) \text{ s.t. } D = \nabla X, Q = \nabla^2 X, Z = \mathcal{H}X. \quad (7)$$

The augmented Lagrangian function of the problem (7) is given as follows:

$$\mathcal{L}(X, Z, D, Q, \rho_1, \rho_2, \rho_3) = \left( \gamma \|D\|_1 + (1-\gamma)\|Q\|_1 + \frac{\lambda_1}{2}\|Z - G\|_2^2 + \lambda_2 \langle 1, Z - G\log Z \rangle \right. \quad (8)$$

$$\left. - \langle \rho_1, D - \nabla X \rangle + \frac{\eta_1}{2}\|D - \nabla X\|_2^2 - \langle \rho_2, Q - \nabla^2 X \rangle + \frac{\eta_2}{2}\|Q - \nabla^2 X\|_2^2 - \langle \rho_3, Z - \mathcal{H}X \rangle + \frac{\eta_3}{2}\|Z - \mathcal{H}X\|_2^2 \right),$$

where $\eta_1$, $\eta_2$, $\eta_3$ - positive parameters; $\rho_1, \rho_2, \rho_3$ - with Lagrangian multipliers.

The minimization problem of $X$ subproblem in (8) is given by:

$$X^{(k+1)} = \arg\min_X \left( -\langle \rho_1, D - \nabla X \rangle + \frac{\eta_1}{2}\|D - \nabla X\|_2^2 - \langle \rho_2, Q - \nabla^2 X \rangle + \frac{\eta_2}{2}\|Q - \nabla^2 X\|_2^2 - \langle \rho_3, Z - \mathcal{H}X \rangle + \frac{\eta_3}{2}\|Z - \mathcal{H}X\|_2^2 \right).$$

Thus, we get:

$$\eta_1 \nabla^T (\nabla X + \frac{\rho_1^{(k)}}{\eta_1} - D^{(k)}) + \eta_2 \nabla^{2^T} (\nabla^2 X + \frac{\rho_2^{(k)}}{\eta_2} - Q^{(k)}) + \eta_3 \mathcal{H}^T (\mathcal{H}X + \frac{\rho_3^{(k)}}{\eta_3} - Z^{(k)}) = 0.$$

Note that $\mathcal{H}^T\mathcal{H}$, $\nabla^T\nabla$, $\nabla^{2^T}\nabla^2$ are block circulant with circulant block under periodic boundary conditions. They can be diagonalized by a 2D discrete Fourier transform [34]. The system is linear, symmetric positive definite, then $X^{(k+1)}$ can be efficiently solved by fast Fourier transform, under the periodic boundary conditions as follows:

$$X^{(k+1)} = \mathcal{F}^{-1}\left( \frac{\mathcal{F}\left( \eta_1 \nabla^T (D^{(k)} - \frac{\rho_1^{(k)}}{\eta_1}) + \eta_2 \nabla^{2^T} (Q^{(k)} - \frac{\rho_2^{(k)}}{\eta_2}) + \eta_3 \mathcal{H}^T (Z^{(k)} - \frac{\rho_3^{(k)}}{\eta_3}) \right)}{\eta_1 \mathcal{F}(\nabla^T\nabla) + \eta_2 \mathcal{F}(\nabla^{2^T}\nabla^2) + \eta_3 \mathcal{F}(\mathcal{H}^T\mathcal{H})} \right), \quad (9)$$

where $\mathcal{F}$ and $\mathcal{F}^{-1}$ are the forward and inverse Fourier transform operators [34].

The $D$ and $Q$ subproblems are given by:

$$D^{(k+1)} = \arg\min_D \left( \gamma \|D\|_1 - \langle \rho_1, D - \nabla X \rangle + \frac{\eta_1}{2}\|D - \nabla X\|_2^2 \right),$$

$$Q^{(k+1)} = \arg\min_Q \left( (1-\gamma)\|Q\|_1 - \langle \rho_2^{(k)}, Q - \nabla^2 X^{(k+1)} \rangle + \frac{\eta_2}{2}\|Q - \nabla^2 X^{(k+1)}\|_2^2 \right).$$

Similarly to [32], the shrinkage formula can be employed for solving the $D$ and $Q$ subproblems as follows:

$$D^{(k+1)} = \text{Shrink}(\nabla X^{(k+1)} + \frac{\rho_1^{(k)}}{\eta_1}, \frac{\gamma}{\eta_1}), \quad (10)$$

$$Q^{(k+1)} = \text{Shrink}(\nabla^2 X^{(k+1)} + \frac{\rho_2^{(k)}}{\eta_2}, \frac{1-\gamma}{\eta_2}), \tag{11}$$

where $\text{Shrink}(y, \varphi) = \frac{y}{|y|} \cdot \max(|y| - \varphi, 0)$.

The $Z$ subproblem is given by:

$$Z^{(k+1)} = \arg\min_{Z} \left( \frac{\lambda_1}{2} \|Z - G\|_2^2 + \lambda_2 \langle 1, Z - G \log Z \rangle - \langle \rho_3^{(k)}, Z - \mathcal{H}X^{(k+1)} \rangle + \frac{\eta_3}{2} \|Z - \mathcal{H}X^{(k+1)}\|_2^2 \right).$$

Therefore, we get:

$$\lambda_1(Z - G) + \lambda_2(1 - \frac{G}{Z}) + \eta_3(Z - \mathcal{H}X^{(k+1)}) - \rho_3^{(k)} = 0.$$

The solution $Z^{(k+1)}$ can be obtained by:

$$Z^{(k+1)} = \frac{(\eta_3 \mathcal{H}X^{(k+1)} + \rho_3^{(k)} - \lambda_2 + \lambda_1 G) + \sqrt{(\eta_3 \mathcal{H}X^{(k+1)} + \rho_3^{(k)} - \lambda_2 + \lambda_1 G)^2 + 4(\eta_3 + \lambda_1)\lambda_2 G}}{2(\eta_3 + \lambda_1)}. \tag{12}$$

Finally, the Lagrangian multipliers $\rho_1^{(k+1)}, \rho_2^{(k+1)}, \rho_3^{(k+1)}$ are updated by the following:

$$\begin{cases} \rho_1^{(k+1)} = \rho_1^{(k)} + \eta_1(\nabla X^{(k+1)} - D^{(k+1)}), \\ \rho_2^{(k+1)} = \rho_2^{(k)} + \eta_2(\nabla^2 X^{(k+1)} - Q^{(k+1)}), \\ \rho_3^{(k+1)} = \rho_3^{(k)} + \eta_3(\mathcal{H}X^{(k+1)} - Z^{(k+1)}). \end{cases} \tag{13}$$

For the choice of edge indication function, there are several methods to the function $\gamma(x)$, see [25, 38]. In experiments, we choose the form of functions $\gamma(x)$ as follows:

$$\gamma_{i,j}(t) = \begin{cases} 1 & \text{if} \frac{|\nabla X_{i,j}^{(k)}|}{\max(|\nabla X^{(k+1)})|} \geq c \\ \frac{1}{2} \cos\left( \frac{2\pi |\nabla X_{i,j}^{(k)}|}{c \max(|\nabla X_{i,j}^{(k+1)}|)} \right) + \frac{1}{2} \end{cases} . \tag{14}$$

As shown in [38], when values $|\nabla X|$ are large or small then the value of $\gamma$ tends to 1, and when intermediate values of $|\nabla X|$ then the value of $\gamma$ is closer to 0. Hence, the value of $c$ must attain its minimum value in linearly sloped regions and its proper value is $c \in (0.05, 0.2)$. We can note that another techniques can be applied to find regularization parameters to get better results. The complete method is described in **Algorithm 1**. The iteration is stopped when the maximum number of allowed outer iterations reaches $\mathcal{N}$ or $ERR = \frac{\|X^{(k)} - X^{(k-1)}\|_2}{\|X^{(k)}\|_2}$ is bigger than tolerance $\varsigma$.

The proposed model is convex (Theorem 1); therefore, the convergence of **Algorithm 1** can be proved by convergence analysis for the alternating minimization method [39]. Hence, based on [28, 36, 40, 41], we have the following theorem:

**Theorem 2** *Given a sequence* $\{X^{(k)}, D^{(k)}, Q^{(k)}, Z^{(k)}, \rho_1^{(k)}, \rho_2^{(k)}, \rho_3^{(k)}\}$ *generated by* ***Algorithm 1****. With any initialization* $\{X^{(0)}, D^{(0)}, G^{(0)}, Z^{(0)}, \rho_1^{(0)}, \rho_2^{(0)}, \rho_3^{(0)}\}$*, the given sequence converges to* $\{X^*, D^*, G^*, Z^*, \rho_1^*, \rho_2^*, \rho_3^*\}$*, where* $X^*$ *is unique solution of the problem* (3)*, and this means* $\lim_{k \to \infty} \|X^{(k)}\|_2 = X^*$.

**Algorithm 1: Algorithm for solving the model (3).**

**Input**: $X^{(0)} = Z^{(0)} = G$; $D^{(0)} = Q^{(0)} = 0$; $k = 1$;
**While** $\Big((ERR > \varsigma)||(k \leq \mathcal{N})\Big)$ **do**
  -Calculate $X^{(k+1)}$ by (9).
  -Calculate $D^{(k+1)}$ by (10).
  -Calculate $Q^{(k+1)}$ by (11).
  -Calculate $Z^{(k+1)}$ by (12).
  -Update $\rho_1^{(k+1)}$, $\rho_2^{(k+1)}$, $\rho_3^{(k+1)}$ by (13).
  -Update $\gamma$ by (14).
  -$k = k + 1$.
**End while**
**Output** $X^* = X^{(k+1)}$.

## 4. Numerical experiments

In this section, we illustrate the performance of the proposed model for MPGN removal. In order to prove the superiority of the proposed model, we compare our results with those of the hybrid higher-order TV model (HOTV)[21] and the MGPTV model defined in Eq. (1). The compared models are implemented by the state-of-the-art alternating minimization algorithm.

All experiments were run on Matlab and Windows 10 with an Intel Core−i5, 2.4 GHz and 8 GB of RAM. For quantitative comparison, we use peak signal-to-noise ratio (PSNR) and the structural similarity index (SSIM) to measure quality of the restoration results. The SSIM measure compares local patterns of pixel intensities normalized for luminance and contrast, and allows us to get more consistent with human visual characteristics [42].

$$PSNR = 10\log_{10}\left(\frac{255^2 \cdot MN}{\|X^* - X\|_2^2}\right),$$

$$SSIM(X, X^*) = \frac{(2\mu_X\mu_{X^*} + c_1)(2\sigma_{X,X^*} + c_2)}{(\mu_X^2 + \mu_{X^*}^2 + c_1)(\sigma_X^2 + \sigma_{X^*}^2 + c_2)},$$

where $X, X^*$ are the original image, the reconstructed or noisy image accordingly; $\mu_X$, $\mu_{X^*}$ are the means of $X$, $X^*$, respectively; $\sigma_X, \sigma_{X^*}$ their standard deviations; $\sigma_{X,X^*}$ the covariance of two images $X$ and $X^*$; $c_1 = (K_1L)^2$; $c_2 = (K_2L)^2$, $L$ is the dynamic range of the pixel values ($L = 255$ for 8-bit grayscale images), $K_1 \ll 1$ , $K_2 \ll 1$. The test images are shown in Figures 1a–1e. Empirically, all images are processed with the equivalent parameters empirically $\lambda = 0.4$, $\beta = 0.6$, $\eta_1 = 1.2$, $\eta_2 = 0.1$, and $\eta_3 = 1$, which gave the best restoration results. We set tolerance $\varsigma = 0.0001$ and the maximum number of iterations $N = 200$.

(a) Cameraman (b) Lighthouse (c) Castle (d) Butterfly (e) Brain

**Figure 1**. Test images.

**First experiment: image denoising**

In this case, $\mathcal{H}$ is an identity matrix. The observed images are simulated by adding Poisson noise using the MATLAB command $poissrnd(X/\sigma_p) * \sigma_p$ and additive Gaussian noise with noise level $\sigma_g$.

The visual performance of compared models for the test images is shown in Figures 2 and 3 with noise levels $\sigma_p = 1$, $\sigma_g = 5$ and is shown in Figures 4 and 5 with noise levels $\sigma_p = 3$, $\sigma_g = 5$. In Figures 2a, 3a, 4a, and 5a, we show the noisy images. In Figures 2b–2d and 4b–4d, we show the reconstructions via HOTV model, MGPTV model and our model, respectively. We also show the zoomed details of original images in Figures 2e and 4e and the zoomed details of the restored images given by the tested methodsi respectivelyi in Figures 2f–2h and 4f–4h. In addition, in Figures 3b-3d and 5b-5d, we show the reconstructions given by tested methods attaching the zoomed details of the restored images. As we see in these figures, the visual quality of the images restored by our model is superior to the images restored by the other models.

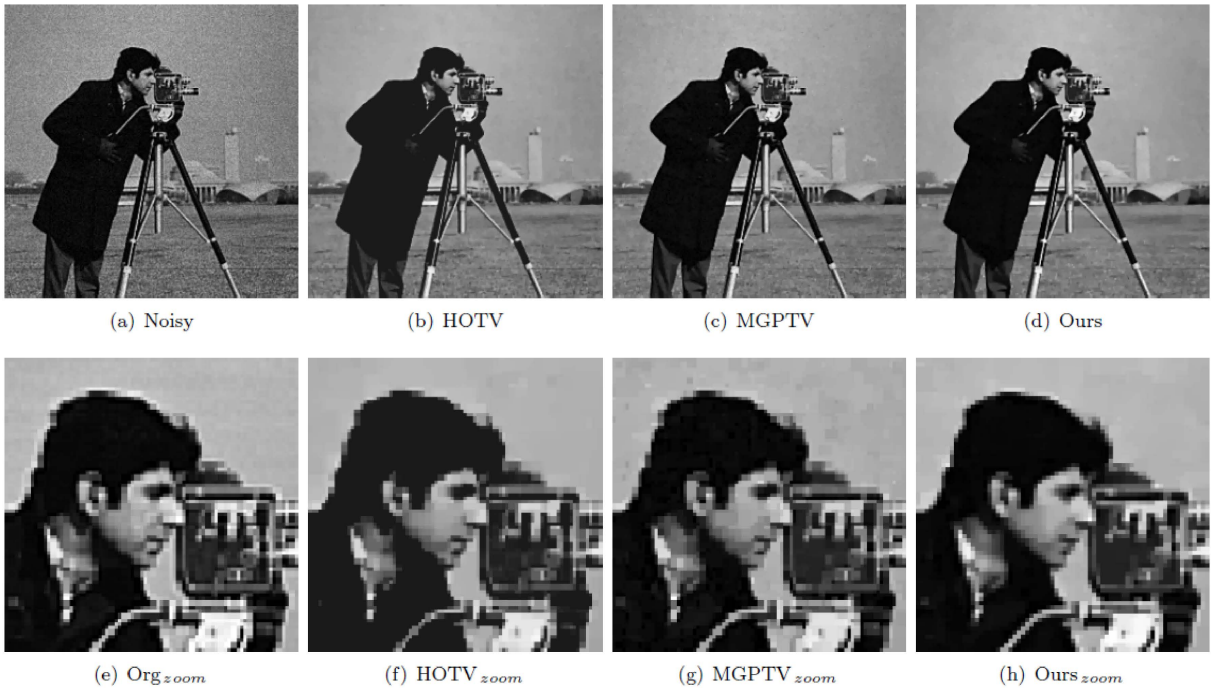

(a) Noisy (b) HOTV (c) MGPTV (d) Ours

(e) Org$_{zoom}$ (f) HOTV$_{zoom}$ (g) MGPTV$_{zoom}$ (h) Ours$_{zoom}$

**Figure 2**. Image 'Cameraman': recovered images of different approaches for image denoising. a) noisy image $G$ with $\sigma_p = 1$, $\sigma_g = 5$; b) restored image by HOTV; c) restored image by MGPTV; d) restored image by our approach.

An important factor to measure the effectiveness of the denoising methods is run time. Table 1 shows the convergence results of all tested algorithms for different images. Furthermore, in Figures 6a–6c, we show the evolution of ERR as a function of the number of iterations for the compared methods. From these figures, we can confirm the convergence behaviour of the compared methods with the error decreased monotonically per iteration. It can be observed from the table that the computation time of the restored images using our model and MGPTV is about the same, and the computation time of the restored images by the proposed method is less than that required by HOTV. In Tables 2 and 3, we show the comparison results in terms of SSIM and PSNR (the best result is highlighted in bold). We can clearly see that our method outperforms the other relative methods for mixed Poisson-Gaussian noise removal.

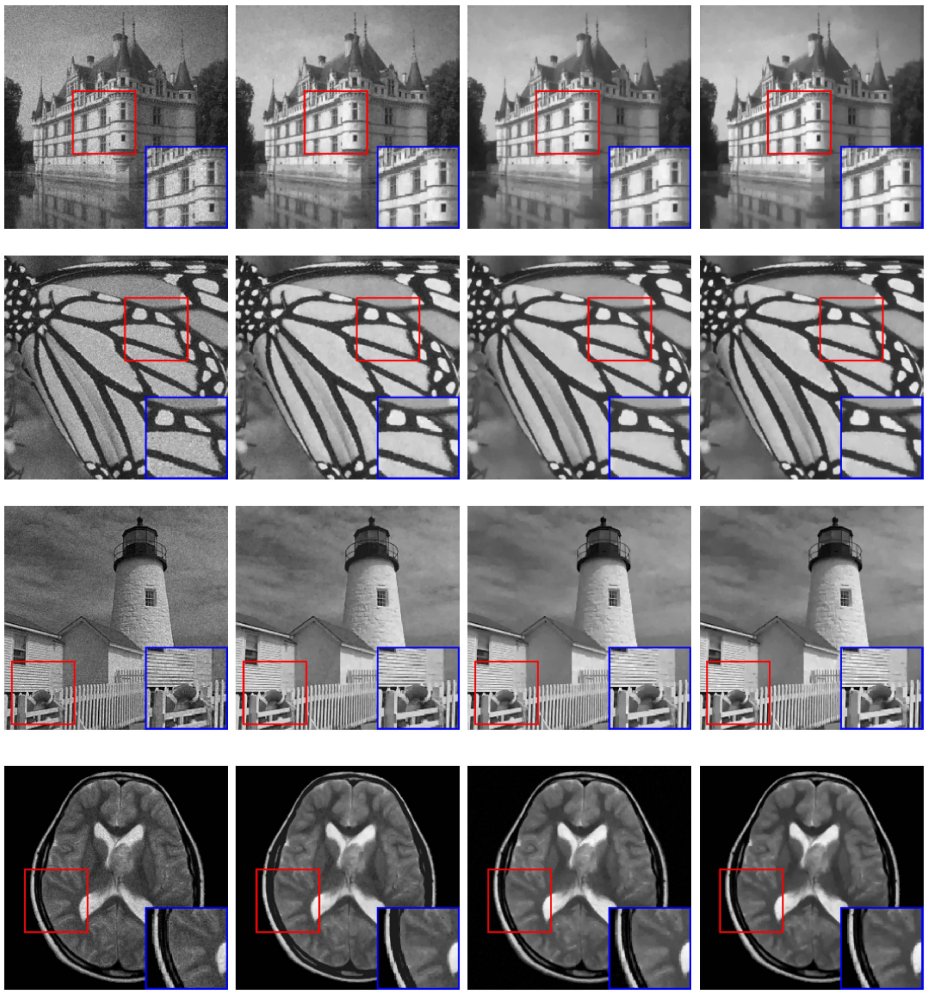


**Figure 3**. Recovered images of different approaches for image denoising. a) noisy image $G$ with $\sigma_p = 1$, $\sigma_g = 5$; b) restored image by HOTV; c) restored image by MGPTV; d) restored image by our approach.

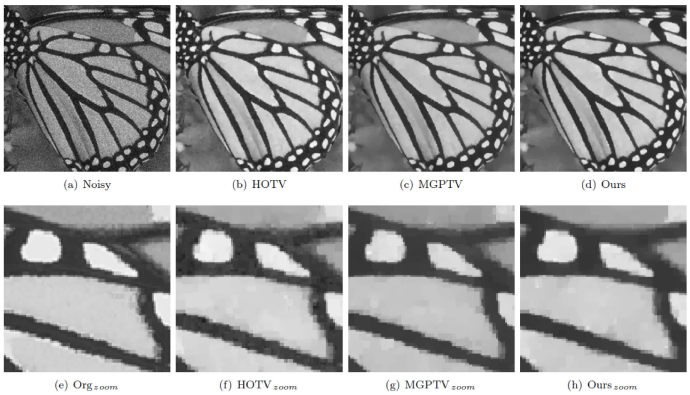


**Figure 4**. Image 'Butterfly': recovered images of different approaches for image denoising. a) noisy image $G$ with $\sigma_p = 1$, $\sigma_g = 5$; b) restored image by HOTV; c) restored image by MGPTV; d) restored image by our approach.

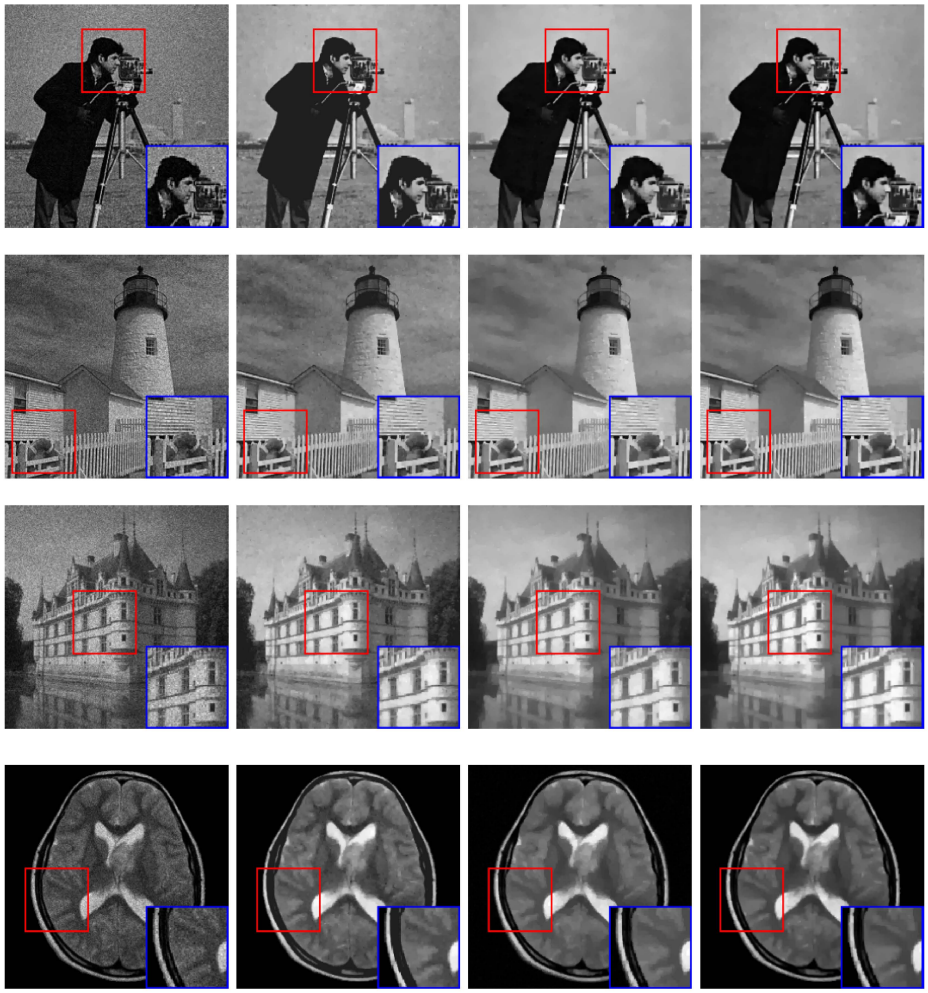

(a) Noisy (b) HOTV (c) MGPTV (d) Ours

**Figure 5**. Recovered images of different approaches for image denoising. a) noisy image $G$ with $\sigma_p = 3$, $\sigma_g = 5$; b) restored image by HOTV; c) restored image by MGPTV; d) restored image by our approach.

**Table 1**. Computational time for image denoising.

| Image | Method | Time (in seconds) | $N_{iter}$ |
|---|---|---|---|
| Castle ($\sigma_g = 1, \sigma_p = 5$) | HOTV | 0.7954 | 28 |
| | MGPTV | 0.6015 | 18 |
| | Ours | 0.6126 | 18 |
| Brain ($\sigma_g = 1, \sigma_p = 5$) | HOTV | 2.3214 | 69 |
| | MGPTV | 1.1220 | 59 |
| | Ours | 1.0423 | 54 |
| Butterfly ($\sigma_g = 3, \sigma_p = 5$) | HOTV | 0.8678 | 23 |
| | MGPTV | 0.7620 | 18 |
| | Ours | 0.7868 | 19 |

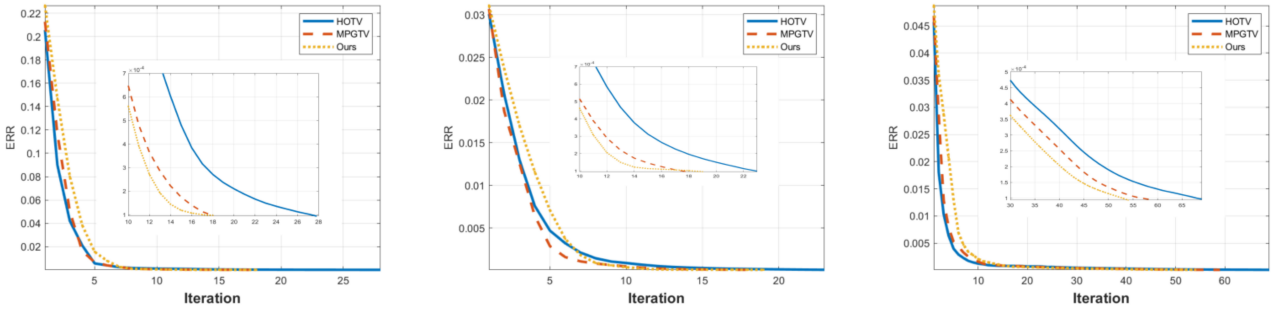


(a) Castle (b) Butterfly (c) Brain

**Figure 6**. Plots of the error values (ERR) versus iterations of the TV-based methods for image denoising.

**Table 2**. PSNR and SSIM values for noisy images and restored images with noise level $\sigma_p = 1$, $\sigma_g = 5$.

| Image | PSNR | | | | SSIM | | | |
|---|---|---|---|---|---|---|---|---|
| | Noisy | HOTV | MGPTV | Ours | Noisy | HOTV | MGPTV | Ours |
| **Cameraman** | 22.6034 | 26.1429 | 28.0327 | **29.6009** | 0.6468 | 0.8304 | 0.8587 | **0.8658** |
| **Lighthouse** | 23.1926 | 27.3772 | 27.8199 | **28.3255** | 0.6741 | 0.8590 | 0.8587 | **0.8678** |
| **Castle** | 18.0378 | 27.6571 | 27.9929 | **28.9437** | 0.6637 | 0.8800 | 0.8852 | **0.8915** |
| **Butterfly** | 20.4104 | 30.3151 | 30.6999 | **31.4352** | 0.7362 | 0.9196 | 0.9386 | **0.9422** |
| **Brain** | 25.6292 | 28.7183 | 31.5635 | **33.0640** | 0.8292 | 0.90176 | 0.8760 | **0.9432** |

**Table 3**. PSNR and SSIM values for noisy images and restored images with noise level $\sigma_p = 3$, $\sigma_g = 5$.

| Image | PSNR | | | | SSIM | | | |
|---|---|---|---|---|---|---|---|---|
| | Noisy | HOTV | MGPTV | Ours | Noisy | HOTV | MGPTV | Ours |
| **Cameraman** | 19.0732 | 25.0359 | 26.3278 | **27.0434** | 0.5178 | 0.7709 | 0.8052 | **0.8123** |
| **Lighthouse** | 16.9552 | 23.2803 | 24.3522 | **24.8347** | 0.5221 | 0.7670 | 0.7801 | **0.7922** |
| **Castle** | 16.4501 | 24.8839 | 25.4574 | **26.9789** | 0.5091 | 0.8123 | 0.8180 | **0.8299** |
| **Butterfly** | 17.2101 | 26.9709 | 27.6911 | **28.8553** | 0.6111 | 0.8930 | 0.9038 | **0.9107** |
| **Brain** | 23.1269 | 27.2700 | 29.8279 | **30.7990** | 0.7374 | 0.8760 | 0.8525 | **0.9089** |

**Second experiment: image deblurring and denoising**

In this case, we perform simultaneously image deblurring and denoising. The blurred image is simulated by Gaussian blur of size $8 \times 8$ with standard deviation of 1. Then the blurred image is contaminated by Poisson noise with $\sigma_p = 3$ and Gaussian noise with $\sigma_g = 5$. In Figures 7a and 8a, we represent the blurred and noisy image. In the others, Figures 7b–7d and 8b–8d separately, we show respectively the reconstructions given by HOTV model, MGPTV model and our model. In these figures, we have enlarged some details of restored images. In Table 4 we also illustrate the convergence results of all tested algorithms for three different images. Besides, in Figures 9a–9c, we show the evolution of ERR as a function of the number of iterations for the compared methods. From the figures, we also confirm the convergence behaviour of the compared methods.

For the comparison of the performance quantitatively, we report the PSNR and SSIM values in Table 5. Visually, it can be seen that our proposed method reaches better visual quality and higher PSNR and

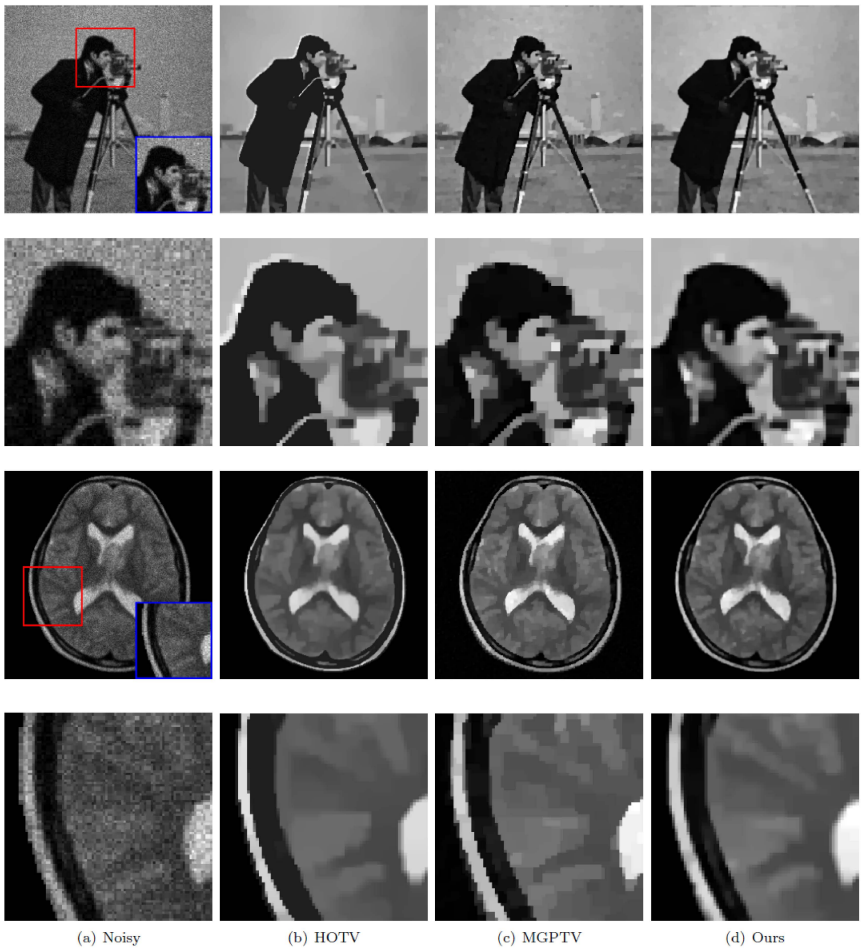


**Figure 7**. Results for images: recovered images of different approaches for image denoising. a) Blurring and noisy image $G$ with $\sigma_p = 3$, $\sigma_g = 5$; b) restored image by HOTV; c) restored image by MGPTV; d) restored image by our approach.

**Table 4**. Computational time for image denoising and debluring.

| Image | Method | Time (in seconds) | $N_{iter}$ |
|---|---|---|---|
| Cameraman | HOTV | 1.9527 | 51 |
| | MGPTV | 1.4894 | 45 |
| | Ours | 1.4170 | 41 |
| Lighthouse | HOTV | 1.4858 | 53 |
| | MGPTV | 1.3870 | 49 |
| | Ours | 1.3062 | 43 |
| Butterfly | HOTV | 1.6731 | 49 |
| | MGPTV | 1.5243 | 45 |
| | Ours | 1.4800 | 42 |

SSIM values. The numerical simulations suggest again the effectiveness of our proposed method for image reconstruction under mixed Poisson-Gaussian noise even in the presence of blur.

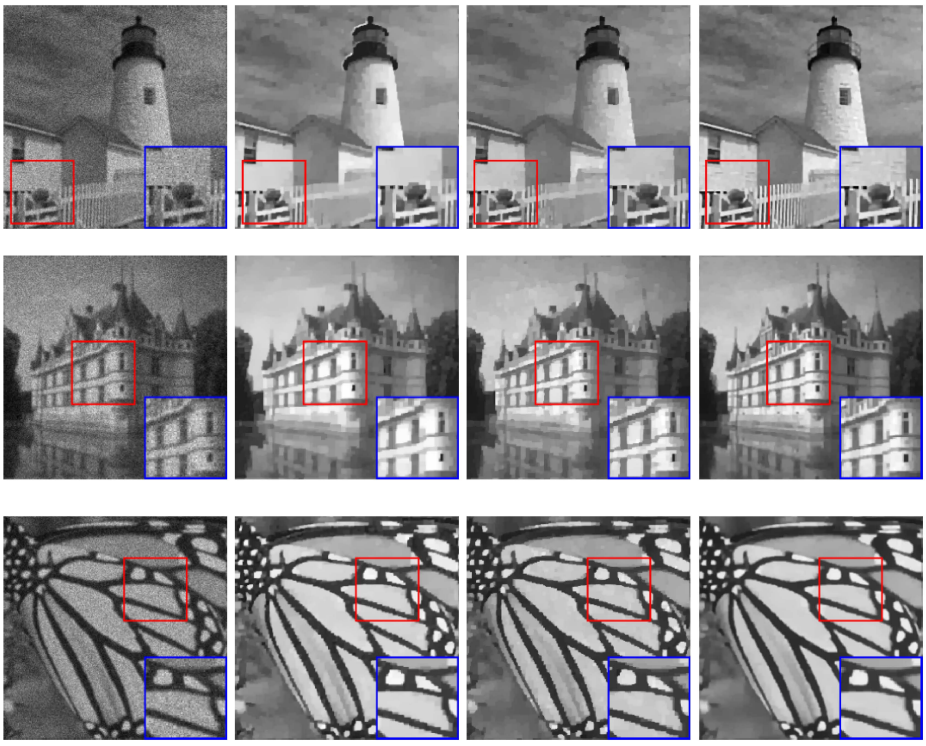

(a) Noisy (b) HOTV (c) MGPTV (d) Ours

**Figure 8**. Results for images: recovered images of different approaches for image denoising. a) blurring and noisy image $G$ with $\sigma_p = 3$, $\sigma_g = 5$; b) restored image by HOTV; c) restored image by MGPTV; d) restored image by our approach.

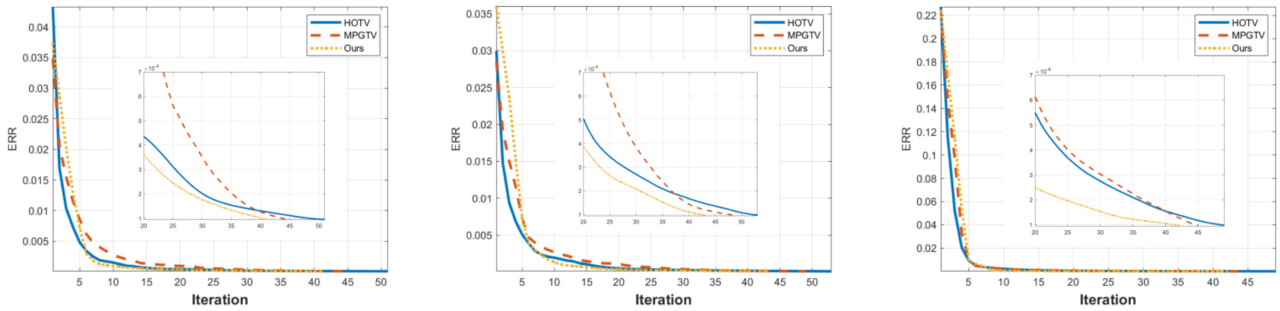


(a) Cameraman (b) Lighthouse (c) Butterfly

**Figure 9**. Plots of the error values (ERR) versus iterations of the TV-based methods for image denoising and debluring.

## Conclusion

In this work, we propose a hybrid regularizer approach which combines the first and second-order TV for denoising and deblurring image corrupted by MPGN. We employ a highly efficient alternating minimization algorithm for solving the optimization problem and compare with two other MPGN removal methods. The experiments demonstrate the superiority of the proposed method. The proposed method removes MPGN noise quite well and overcomes staircase effect caused by total variation regularization. In our paper, the limitation of the proposed method is that we do not update the regularization parameters during the iteration. In future research, we would like to overcome the issue and apply the proposed method to different noise models.

**Table 5**. PSNR and SSIM values for blurring and noisy images and restored images with noise level $\sigma_p = 3$, $\sigma_g = 5$.

| **Image** | **PSNR** | | | | **SSIM** | | | |
|---|---|---|---|---|---|---|---|---|
| | **Noisy** | **HOTV** | **MGPTV** | **Ours** | **Noisy** | **HOTV** | **MGPTV** | **Ours** |
| **Cameraman** | 18.8795 | 20.6446 | 21.7991 | **23.2953** | 0.3434 | 0.6428 | 0.6979 | **0.7397** |
| **Lighthouse** | 15.8398 | 18.7710 | 19.3424 | **20.3709** | 0.2764 | 0.5863 | 0.5898 | **0.6317** |
| **Castle** | 15.8086 | 23.7668 | 23.7720 | **24.4558** | 0.3617 | 0.7132 | 0.7100 | **0.7587** |
| **Butterfly** | 17.2880 | 21.9563 | 22.2856 | **24.5585** | 0.4958 | 0.8257 | 0.8086 | **0.8660** |
| **Brain** | 22.3658 | 23.7707 | 24.8696 | **27.9999** | 0.6633 | 0.7697 | 0.7452 | **0.8735** |

**Acknowledgments**

The authors would like to thank the editor and anonymous referees for their insightful comments and suggestions. This research is funded by Funds for Science and Technology Development of the University of Danang under project number B2019-DN03-46.

## References

[1] Jezierska A, Pesquet JC, Talbot H, Chaux C. Iterative Poisson-Gaussian noise parametric estimation for blind image denoising. In: International Conference on Image Processing (ICIP); Paris, France; 2014. pp. 2819-2823.

[2] Le T, Chartrand R, Asaki TJ. A variational approach to reconstructing images corrupted by Poisson noise. Journal of Mathematical Imaging and Vision 2007; 27 (3): 257-263. https://doi.org/10.1007/s10851-007-0652-y

[3] Li J, Luisier F, Blu T. PURE-LET Image Deconvolution. IEEE Transactions on Image Processing 2018; 27 (1): 92-105. https://doi.org/10.1109/TIP.2017.2753404

[4] Pham CT, Kopylov AV. Tree-serial parametric dynamic programming with flexible prior model for image denoising. Computer Optics 2018; 42 (5): 838-845. https://doi.org/10.18287/2412-6179-2018-42-5-838-845

[5] Benvenuto F, Camera AL, Theys C, Ferrari A, Lantéri H et al. The study of an iterative method for the reconstruction of images corrupted by Poisson and Gaussian noise. Inverse Problems 2008; 24 (3): 035016, 20 pages. https://doi.org/10.1088/0266-5611/28/6/069502

[6] Chouzenoux E, Jezierska A, Pesquet JC, Talbot H. A convex approach for image restoration with exact Poisson-Gaussian likelihood. SIAM Journal on Imaging Sciences 2015; 8 (4): 2662-2682. https://doi.org/10.1137/15M1014395

[7] Delpretti S, Luisier F, Ramani S, Blu T, Unser M. Multiframe sure-let denoising of timelapse fluorescence microscopy images. In: IEEE 5th International Symposium on Biomedical Imaging: From Nano to Macro; Paris, France; 2008. pp. 149-152.

[8] Lanza A, Morigi S, Sgallari F, Wen YW. Image restoration with Poisson-Gaussian mixed noise. Computer Methods in Biomechanics and Biomedical Engineering: Imaging & Visualization 2013; 2 (1): 12-24. https://doi.org/10.1080/21681163.2013.811039

[9] Gao Q, Eck S, Matthias J, Chung I, Engelhardt J et al. Bayesian joint super-resolution, deconvolution, and denoising of images with Poisson-Gaussian noise. In: IEEE 15th International Symposium on Biomedical Imaging; Washington, DC, USA; 2018. pp. 938-942.

[10] Le Montagner Y, Angelini ED, Olivo-Marin JC. An unbiased risk estimator for image denoising in the presence of mixed Poisson–Gaussian noise. IEEE Transactions on Image Processing 2014; 23 (3): 1255–1268. https://doi.org/10.1109/TIP.2014.2300821

[11] Li J, Shen Z, Yin R, Zhang X. A reweighted $l^2$ method for image restoration with Poisson and mixed Poisson-Gaussian noise. Inverse Problems and Imaging 2015; 9 (3): 875-894. https://doi.org/10.3934/ipi.2015.9.875

[12] Marnissi Y, Zheng Y, Pesquei JC. Fast variational Bayesian signal recovery in the presence of Poisson-Gaussian noise. In: IEEE International Conference on Acoustics, Speech and Signal Processing; Shanghai, China; 2016. pp. 3964-3968.

[13] Pham CT, Gamard G, Kopylov A, Tran TTT. An algorithm for image restoration with mixed noise using total variation regularization. Turkish Journal of Electrical Engineering & Computer Sciences 2018; 26 (6): 2831-2845. https://doi.org/10.3906/elk-1803-100

[14] Bohra P, Garg D, Gurumoorthy KS, Rajwade A. Variance-stabilization-based compressive inversion under Poisson or Poisson–Gaussian noise with analytical bounds. Inverse Problems 2019; 35 (10): 105006, 34 pages. https://doi.org/10.1088/1361-6420/ab2aa7

[15] Yang S, Lee BU. Poisson-Gaussian Noise Reduction Using the Hidden Markov Model in Contourlet Domain for Fluorescence Microscopy Images. PLoS ONE 2015; 10 (9): e0136964, 19 pages. https://doi.org/10.1371/journal.pone.0136964

[16] Calatroni L, De Los Reyes J, Schronlieb C. Infimal Convolution of Data Discrepancies for Mixed Noise Removal. SIAM Journal on Imaging Sciences 2017; 10 (3): 1196-1233. https://doi.org/10.1137/16M1101684

[17] De Los Reyes JC, Schonlieb CB. Image denoising: Learning the noise model via nonsmooth PDE-constrained optimization. Inverse Problems and Imaging 2013; 7 (4): 1183-1214. https://doi.org/10.3934/ipi.2013.7.1183

[18] Liu J, Huang TZ, Xu Z, Lv XG. High-order total variation-based multiplicative noise removal with spatially adapted parameter selection. Journal of the Optical Society of America A 2013; 30 (10): 1956-1966. https://doi.org/10.1364/JOSAA.30.001956

[19] Kayyar SH, Jidesh P. Non-local total variation regularization approach for image restoration under a Poisson degradation. Journal of Modern Optics 2018; 65 (19): 2231–2242. https://doi.org/10.1080/09500340.2018.1506058

[20] Ma M, Zhang J, Deng C, Liu Z, Wang Y. Adaptive Image Restoration via a Relaxed Regularization of Mean Curvature. Mathematical Problems in Engineering 2020; 2020: 416907, 11 pages. https://doi.org/10.1155/2020/3416907

[21] Jiang L, Huang J, Lv XG, Liu J. Alternating direction method for the high-order total variation-based Poisson noise removal problem. Numerical Algorithms 2015; 69 (3): 495-516. https://doi.org/10.1007/s11075-014-9908-y

[22] Chen HZ, Song JP, Tai XC. A dual algorithm for minimization of the LLT model. Advances in Computational Mathematics 2009; 31: 115-130. https://doi.org/10.1007/s10444-008-9097-0

[23] Papafitsoros K, Schönlieb CB. A combined first and second order variational approach for image reconstruction. Journal of Mathematical Imaging and Vision 2014; 48: 308-338. https://doi.org/10.1007/s10851-013-0445-4

[24] Aubert G, Kornprobst P. Mathematical Problems in Image Processing: partial differential equations and the calculus of variations. Applied Mathematical Science 147. 2nd ed. New York, USA: Springer-Verlag, 2008.

[25] Li F, Shen CM, Fan JS, Shen CL. Image restoration combining a total variational filter and a fourth-order filter. Journal of Visual Communication and Image Representation 2007; 18 (4): 322-330. doi: https://doi.org/10.1016/j.jvcir.2007.04.005

[26] Osher S, Scherzer O. G-norm properties of bounded variation regularizations. Communications in Mathematical Sciences 2004; 2 (2): 237-254. https://doi.org/10.4310/CMS.2004.v2.n2.a6

[27] Jiang L, Huang J, Lv XG, Liu J. Restoring Poissonian Images by a Combined First-Order and Second-Order Variation Approach. Journal of Mathematics 2013; 2013: 274573, 11 pages. https://doi.org/10.1155/2013/274573

[28] Zhang J, Ma M, Wu Z, Deng C. High-Order Total Bounded Variation Model and Its Fast Algorithm for Poissonian Image Restoration.Mathematical Problems in Engineering 2019; 2019: 2502731, 11 pages. https://doi.org/10.1155/2019/2502731

[29] Chen YM, Wunderli T. Adaptive total variation for image restoration in BV space. Journal of Mathematical Analysis and Application 2002; 272 (1): 117-137. https://doi.org/10.1016/S0022-247X(02)00141-5

[30] Feinberg EA, Kasyanov PO, Zadoianchuk NV. Fatou's Lemma for Weakly Converging Probabilities. Theory of Probability & Its Applications 2014; 58 (4): 683-689. https://doi.org/10.1137/S0040585X97986850

[31] Chambolle A. An algorithm for total variation minimization and applications. Journal of Mathematical Imaging and Vision 2004; 20: 89-97. https://doi.org/10.1023/B:JMIV.0000011325.36760.1e

[32] Goldstein T, Osher S. The split Bregman method for L1-regularized problems. SIAM Journal on Imaging Sciences 2008; 2 (2): 323–343. https://doi.org/10.1137/080725891

[33] Chan SH, Khoshabeh R, Gibson KB, Gill PE, Nguyen TQ. An Augmented Lagrangian Method for Total Variation Video Restoration. IEEE Transactions on Image Processing 2011; 20 (11): 3097-3111. https://doi.org/10.1109/TIP.2011.2158229

[34] Wang Y, Yang J, Yin W, Zhang Y, A New Alternating Minimization Algorithm for Total Variation Image Reconstruction. SIAM Journal on Imaging Sciences 2008; 1 (3): 248-272. https://doi.org/10.1137/080724265

[35] Wu C, Tai XC. Augmented Lagrangian method, dual methods, and split Bregman iteration for ROF, vectorial TV, and high order models. SIAM Journal on Imaging Sciences 2010; 3 (3): 300–339. https://doi.org/10.1137/090767558

[36] Boyd S, Parikh N, Chu E, Peleato B, Eckstein J. Distributed optimization and statistical learning via the alternating direction method of multipliers. Foundations and Trends in Machine Learning 2010; 3 (1): 1-122. https://doi.org/10.1561/2200000016

[37] Liu X, Huang L. Poissonian image reconstruction using alternating direction algorithm. Journal of Electronic Imaging 2013; 22 (3): 033007, 9 pages. https://doi.org/10.1117/1.JEI.22.3.033007

[38] Lysaker M, Tai XC. Iterative image restoration combining total variation minimization and a second-order functional. International Journal of Computer Vision 2006; 66: 5-18. https://doi.org/10.1007/s11263-005-3219-7

[39] Eckstein J, Bertsekas DP. On the Douglas—Rachford splitting method and the proximal point algorithm for maximal monotone operators. Mathematical Programming 1992; 55: 293-318. https://doi.org/10.1007/BF01581204

[40] He C, Hu C, Zhang W, Shi B. A Fast Adaptive Parameter Estimation for Total Variation Image Restoration. IEEE Transactions on Image Processing 2014; 23 (12): 4954-4967. https://doi.org/10.1109/TIP.2014.2360133

[41] Woo H, Yun S. Alternating Minimization Algorithm for Speckle Reduction With a Shifting Technique. IEEE Transactions on Image Processing 2012; 21: 1701-1714. https://doi.org/10.1109/TIP.2011.2176345

[42] Bovik AC, Wang Z. Modern Image Quality Assessment, Synthesis Lectures on Image, Video, and Multimedia Processing. USA: Morgan and Claypool Publishers, 2006.